Cell

A Regulatory Archipelago Controls *Hox* Genes Transcription in Digits

Thomas Montavon,[1] Natalia Soshnikova,[2] Bénédicte Mascrez,[2] Elisabeth Joye,[1] Laurie Thevenet,[2] Erik Splinter,[3] Wouter de Laat,[3] François Spitz,[4] and Denis Duboule[1,2,*]
[1]National Research Centre, Frontiers in Genetics, School of Life Sciences, Ecole Polytechnique Fédérale, Lausanne, Switzerland
[2]Department of Genetics and Evolution, University of Geneva, Switzerland
[3]Hubrecht Institute-KNAW & University Medical Center Utrecht, Uppsalalaan 8, 3584 CT, Utrecht, The Netherlands
[4]Developmental Biology Unit, EMBL, Heidelberg, Germany
*Correspondence: denis.duboule@unige.ch
DOI 10.1016/j.cell.2011.10.023

SUMMARY

The evolution of digits was an essential step in the success of tetrapods. Among the key players, *Hoxd* genes are coordinately regulated in developing digits, where they help organize growth and patterns. We identified the distal regulatory sites associated with these genes by probing the three-dimensional architecture of this regulatory unit in developing limbs. This approach, combined with in vivo deletions of distinct regulatory regions, revealed that the active part of the gene cluster contacts several enhancer-like sequences. These elements are dispersed throughout the nearby gene desert, and each contributes either quantitatively or qualitatively to *Hox* gene transcription in presumptive digits. We propose that this genetic system, which we call a "regulatory archipelago," provides an inherent flexibility that may partly underlie the diversity in number and morphology of digits across tetrapods, as well as their resilience to drastic variations.

INTRODUCTION

Patterning of the animal body plan largely relies on the function of *Hox* genes. In mammals, four *Hox* gene clusters exist, *HoxA* to *HoxD*, which contain 39 genes altogether. These genes are transcribed sequentially, in both time and space, following their respective positions within each cluster (temporal and spatial colinearities, see Kmita and Duboule, 2003). In the vertebrate lineage, the constraint imposed on gene clustering by the implementation of this ancestral mechanism provided the grounds for evolving additional, cluster-wide regulations, whereby several neighboring genes were coopted along with the emergence of an evolutionary novelty. For example, while *Hoxc* cluster genes are important for the development of hairs (Godwin and Capecchi, 1998), *Hoxd* genes were coopted along with the appearance of limbs (Dollé et al., 1989).

The coordinated transcription of *Hoxd* genes in limb buds is necessary for the development of both the proximal and distal limb segments (Zakany and Duboule, 2007) and follows two independent phases (Nelson et al., 1996; Tarchini and Duboule, 2006), controlled by distinct enhancer systems located on either side of the gene cluster (Spitz et al., 2005). An initial phase of transcription takes place during early limb budding and involves the activation of 3′-located genes (starting with *Hoxd1*). This phase is critical for the patterning of both the arm and forearm, and depends upon enhancer sequences located on the telomeric side of the gene cluster. A second wave of transcription occurs in the most distal part of the limb, concomitantly with digit formation. During this late phase, only *Hoxd13* to *Hoxd10* are transcribed with progressively lower efficiencies, such that *Hoxd13* is expressed at highest levels in all digits, whereas *Hoxd12*, *Hoxd11*, and *Hoxd10* are excluded from the thumb (Montavon et al., 2008). This phase is controlled by enhancer sequences lying centromeric from *Hoxd13* (Spitz et al., 2003; 2005; Tschopp and Duboule, 2011). The existence of distinct regulatory modules suggests that proximal and distal limb structures have different evolutionary histories. Understanding the underlying mechanisms may thus help to reconstitute the evolution of these regulations, which were critical for the emergence and radiation of tetrapods.

Transgenic analyses of this centromeric regulatory landscape identified two enhancer elements, referred to as conserved sequences B (CsB) and CsC (Spitz et al., 2003; Gonzalez et al., 2007), capable of driving reporter gene expression in digits. CsB is part of a Global Control Region (GCR) conserved in all vertebrates and containing various enhancers. It is located 180 kb upstream *Hoxd13*, in a 600 kb large gene desert extending from *Lunapark (Lnp)* until *Atp5g3* (Figure 1A). CsC is part of the Prox enhancer, located between *Lnp* and *Evx2* (Gonzalez et al., 2007), which are both coexpressed with *Hoxd* genes in digits as a bystander effect (Spitz et al., 2003). The combined effect of CsB and CsC was proposed to be required for proper activation of *Hoxd* genes in digits (Gonzalez et al., 2007). However, whether or not these two enhancers are sufficient remained to be assessed, particularly under physiological conditions in vivo.

Distal enhancers often activate transcription of target promoters after physical association via chromatin loops (Bulger and Groudine, 2011). The frequency of specific DNA-DNA

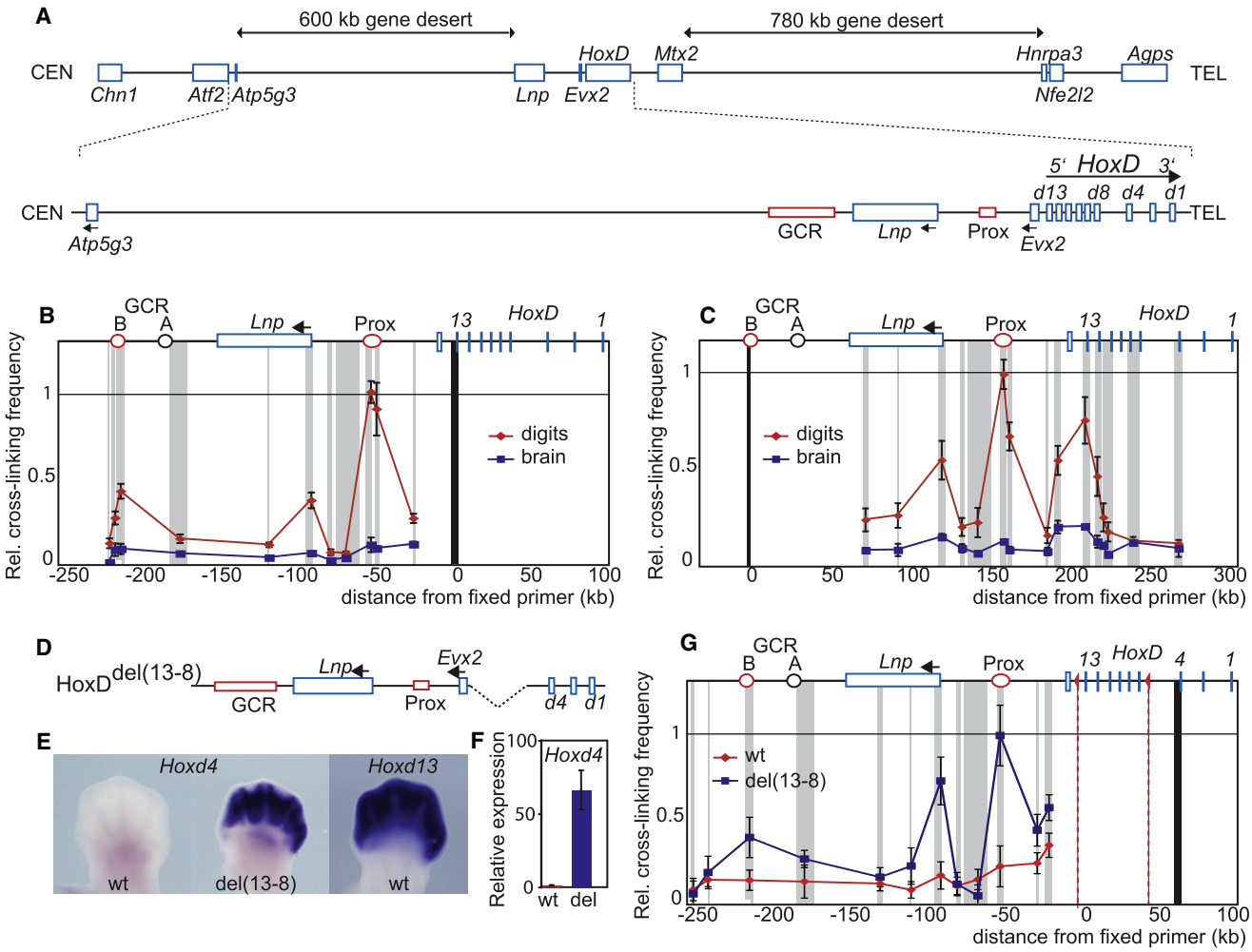

Figure 1. Regulatory Interactions from *Hoxd13* in Developing Digits

(A) The *HoxD* cluster and associated gene deserts (top) with enlarged centromeric region (bottom). The GCR and Prox sequences are in red.

(B) 3C analysis with a *Hoxd13* primer (black bar) tested against primers located at various positions (gray bars). Peak profiles are shown for embryonic digit (red) or brain (blue) material. The highest crosslinking frequency value is set to 1. Error bars indicate SD (n = 3).

(C) Same as in (B) but with a fixed primer located in the CsB of the GCR (black bar). Error bars indicate SD (n = 3).

(D) Scheme of the Del(*8-13*) deletion, with *Hoxd4* now at the extremity of the *HoxD* cluster.

(E) *Hoxd4* is not expressed in E12.5 wild-type limbs (left), unlike in digits of Del(*8-13*) embryos (middle). Wild-type *Hoxd13* expression is shown as control (right).

(F) RT-qPCR quantification of *Hoxd4* expression in E12.5 wild-type and Del(*8-13*) digits. Error bars indicate SD (n = 4).

(G) 3C analysis to compare the locus conformation in wild-type (red) or Del(*8-13*) (blue) digits. The fixed primer maps to the *Hoxd4* promoter (black bar). The red dashed lines indicate the deleted segment. Error bars indicate SD (n = 3).

See also Figure S1.

interactions can be estimated by using Chromosome Conformation Capture (3C) techniques and variants thereof (Dekker et al., 2002; see van Steensel and Dekker, 2010). In this way, chromatin loops were described in various contexts, including the activation of *globin* genes by the upstream Locus Control Region (LCR) and the control of *Sonic hedgehog (Shh)* transcription in early limb buds by a remote enhancer (Tolhuis et al., 2002; Amano et al., 2009).

Here, we show that both the GCR and Prox sequences associate with *Hoxd* genes in presumptive digits in vivo. However, these contacts are not sufficient to elicit the expected transcriptional activation. By combining multiple biochemical and genetic approaches, we identify several DNA segments, spanning the entire gene desert, which are required for a full transcriptional response. This regulatory complexity suggests an explanation for why digit patterning is highly flexible among tetrapods, while, at the same time, digits are very resilient to genetic variation. Modifications within this regulatory archipelago can directly impact digit morphology, thus providing a basis for the diversity in the shapes and numbers of digits in various tetrapods or in human genetic syndromes.

RESULTS

Enhancer-Promoter Interactions at the *HoxD* Locus in Digits

We looked at enhancer-promoter interactions using Chromosome Conformation Capture (3C). The analysis was performed on dissected distal limb buds at embryonic day 12.5 (E12.5), using primers mapping both within and upstream the *HoxD* cluster, covering a DNA segment 350 kilobases (kb) large. Age-matched embryonic fore brains, where *Hox* genes are not expressed, were used as control.

With the *Hoxd13* promoter as a reference point, we observed local peaks of interactions with the GCR and Prox elements in developing digits. Both sequences contacted *Hoxd13* with a frequency higher than neighboring DNA segments (Figure 1B), *Hoxd13* forming stronger interactions with Prox than with the GCR. These contacts were not seen in brain, suggesting a tissue-specific chromosome conformation. *Hoxd13* also interacted with the *Lnp* promoter in digits, yet not in brain, raising the possibility that both genes be contacted simultaneously, rather than alternatively, by shared regulatory elements. The same results were obtained either in E11.5 or in E13.5 distal limbs (Figure S1 available online).

In the reciprocal experiment, we looked for sequences contacting CsB, the element within the GCR carrying digit enhancer activity (Gonzalez et al., 2007). CsB showed interactions with the promoter of *Lnp,* as well as with the 5′ extremity of the *HoxD* cluster (Figure 1C) in digits. The crosslinking frequency was highest for the *Evx2*/*Hoxd13* region and progressively decreased for *Hoxd12* and *Hoxd11*, to reach background levels for *Hoxd8*, thus matching expression levels in digits. A strong association was observed with the Prox element (Figure 1C). In brain, modest interactions were detected when compared to background signals. These various interactions were also observed at E11.5 and E13.5 (Figure S1). We next used Prox or the *Lnp* promoter as reference fragments (Figure S1) and observed contacts with the GCR, *Lnp, Evx2*/*Hoxd13*, or with the GCR, Prox, and *Hoxd13*, respectively. Therefore, each of the GCR, *Lnp*, Prox and *Hoxd13* sequences showed contacts with the three others, suggesting a complex chromosomal architecture associated with *Hox* gene activation in digits.

We assessed the relevance of these interactions by using a deletion of the *Hoxd13* to *Hoxd8* DNA segment [Del(*8-13*)]. In this configuration, *Hoxd4*, which is normally not expressed in digits, becomes ectopically expressed there, much like *Hoxd13* in the wild-type situation (Figures 1D–1F). A fixed primer located in the *Hoxd4* promoter showed no significant contact with centromeric-located sequences in wild-type digits (Figure 1G). In contrast, strong interactions were observed between *Hoxd4* and the GCR, *Lnp* and Prox in mutant digits. Also, the interactions between CsB and either *Lnp* or the Prox element were identical between mutant and wild-type digits (Figure S1G). In contrast, a substantial increase in interaction frequencies was scored between the GCR and the 3′ part of the cluster including the *Hoxd4* gene, when Del(*8-13*) mutant digits were used, pointing to an association between *Hoxd4* and the GCR in parallel with the ectopic expression of this gene.

Several Distal Enhancers Are Necessary for Transcription in Digits

We checked the bidirectionality of these enhancer sequences by introducing a *Hoxd9LacZ-loxP* transgene 28 kb centromeric to the GCR in the gene desert (Figure 2A; *rel5*). When randomly integrated, the same *Hoxd9LacZ* transgene was never expressed in developing limbs (van der Hoeven et al., 1996). However, its recombination upstream the GCR elicited transcription in digits, similar to the expression of *Lnp*, *Evx2* and posterior *Hoxd* genes (Figure 2B, top).

To assess whether the GCR and Prox are sufficient to regulate *Hoxd* gene in digits, we used the *loxP* site in the recombined *Hoxd9LacZ* transgene to engineer a large chromosomal inversion via STRING (Spitz et al., 2005). The second *loxP* site was located 2.7 Mb centromeric of *rel5,* within the *Itga6* gene (Gimond et al., 1998; Figure 2A). This Inv(*rel5-Itga6*) allele did not interrupt the linkage between the GCR, Prox and the *HoxD* cluster, yet it separated them from upstream sequences by a large distance. It also replaced the gene desert by a gene-dense region immediately upstream the GCR.

Unexpectedly, the inverted *Hoxd9LacZ* transgene, now relocated nearly 3 Mb away from both the GCR and Prox, was still expressed in developing digits (Figure 2B). To rule out that this was due to very long distance interactions with either the GCR or Prox, we used 3C to monitor the contacts involving the transgene insertion site (Figure 2C). In the wild-type situation, this sequence showed only weak contacts with the GCR, Prox and *Hoxd13*. In contrast, strong interactions were scored between these various sites in *rel5* mutant digits, in agreement with the expression of the *Hoxd9LacZ* gene in digits (Figure 2C; *rel5*). After inversion, however, the contacts between the *rel5* position and either the GCR, Prox or *Hoxd13* were down to background values (Figure 2C; *inv*), as if the transgene had lost its association with the GCR and Prox, while being still expressed in developing digits. This result suggested that additional regulatory elements, still associated with the transgene after inversion, were thus located centromeric to the *rel5* position, in the gene desert.

Furthermore, animals homozygous for the inversion had shorter digits at birth, with phalanges missing or fused, similar to the deletion of *Hoxd8* to *Hoxd13* (Figure 2D). We looked at *Hoxd* gene expression in wild-type versus inverted embryos and observed a strong downregulation of *Hoxd13* to *Hoxd10* in developing digits from the inverted stock (Figure 2E). While the distal expression of *Hoxd13* to *Hoxd10* was markedly reduced, *Hoxd11* and *Hoxd10* were still expressed in the proximal limb domain as in wild-type controls (Figure 2E), indicating that this regulatory effect did not affect the early phase of expression.

We quantified these changes by RT-qPCR and *Hoxd13* transcripts were reduced to 10% of wild-type levels in *inv* mutant digits, whereas *Hoxd12* to *Hoxd10* were down to 15% to 20% (Figure 2E and Table S1). *Evx2* transcription was virtually abolished, yet *Lnp* was less affected (40% of control). This dramatic effect indicated that the local conformation of the locus was altered in the inverted configuration. Accordingly, the interaction frequency between *Hoxd13* and either the GCR, Prox or *Lnp* in *inv* mutant digits, was severely reduced (Figure 2F). We verified that those genes relocated close to the GCR, after inversion, did not titrate enhancer activity (Figure S2) and thus concluded

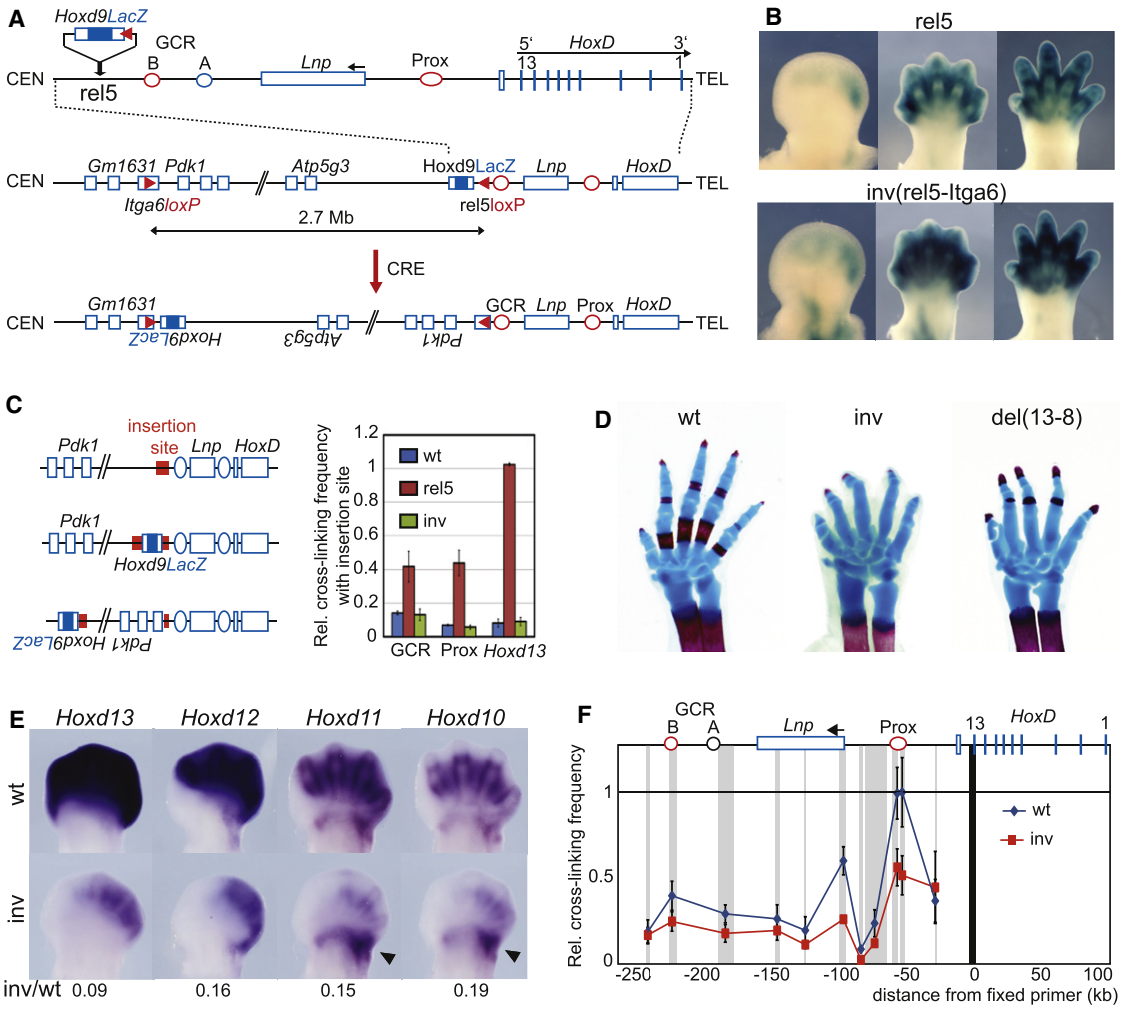

Figure 2. Expression of *Hoxd* Genes in Digits Requires the Proximity of the Gene Desert

(A) Inversion of the centromeric gene desert. A *Hoxd9LacZ* transgene (blue) carrying a *loxP* site (red triangle) was recombined 28 kb centromeric to the GCR (*rel5*, top) and subsequently brought in *cis* with a *loxP* site in the *Itga6* gene (middle). Cre-mediated recombination produced a 2.7 Mb large inversion [Inv(*rel5-Itga6*); bottom].

(B) *LacZ* staining for both noninverted (*rel5*; top) and inverted [Inv(*rel5-Itga6*; bottom] alleles, at E11.5, E13.5, and E14.5. The reporter transgene is active in both configurations.

(C) 3C analysis with a primer located at the recombination site of the *Hoxd9LacZ* transgene (red square in the left panel) in WT (top), noninverted (middle), and inverted (bottom) alleles. *Rel5* digits show increased interactions between *Rel5* and both the GCR, Prox, and *Hoxd13* (red bars; right panel). These contacts are abrogated after inversion (green bars). Error bars indicate SD (n = 2).

(D) Mice homozygous for the inversion display digit alterations at birth (middle), similar to those associated with the deletion of *Hoxd13* to *Hoxd8* (right).

(E) *Hoxd* gene expression in wild-type (top) and inverted (bottom) E12.5 limbs. RT-qPCR quantifications in *inv* digits are indicated below each panel (wild-type levels are set to 1). Arrowheads point to the proximal expression domain of both *Hoxd11* and *Hoxd10*.

(F) 3C analysis with a fixed primer in *Hoxd13*, showing interactions in digits from either wild-type (blue) or inverted (red) specimen. Error bars indicate SD (n = 3). See also Figure S2.

that the inversion separated the locus from as yet undefined upstream enhancers. Accordingly, interactions between the GCR, Prox and *Hoxd* gene promoters, while necessary for the full transcriptional regulation of the locus, are not sufficient.

Organization of the *HoxD* Locus in Digits

We produced profiles of both *Hoxd13* and *Hoxd4* interactions by using 4C (Simonis et al., 2006; Zhao et al., 2006) and high-density tiling microarrays. Most of the interactions were observed in *cis*, within a 2 Mb large domain surrounding the *HoxD* cluster (Figure S3A). Interestingly, contacts largely mapped within the *Atp5g3-Hnrpa3* interval, a region containing range of highly conserved noncoding sequences lying into two gene deserts on either side of the *HoxD* cluster (Lee et al., 2006a; Figure S3B).

In developing digits, *Hoxd13* expectedly displayed interaction peaks (enrichment > 3, $\log_2$ scale) with both Prox and *Lnp*, as well as peaks of lower intensity (enrichment > 2) within the

GCR (Figure 3A). The profile of *Hoxd13* in the brain showed some contacts with the GCR, yet enrichment score and peaks number were low (Figure 5D). Furthermore, *Hoxd13* showed many additional peaks in the *Atp5g3-Hnrpa3* interval (Figure 3A). In digits, 75 out of 83 peaks (90%) occurred on the centromeric side of the *HoxD* cluster, whereas only few significant contacts were scored on the telomeric side (Figure 3B; $p = 2.0 \times 10^{-8}$, Fisher's Exact Test). The profile in brain also showed this bias toward the centromeric side (68 out of 87 peaks, 78%, $p = 2.4 \times 10^{-4}$; Figures 3A and 3B). However, while 28 peaks were shared between both samples, 47 and 40 peaks were specific to digits and brain, respectively.

We asked whether this centromeric bias in *Hoxd13* contacts was gene-specific or reflected a generic architectural feature of the locus and mapped the *Hoxd4* interaction profile, a gene transcriptionally silent in developing digits. A strikingly different profile was observed, with the majority of contacts involving the telomeric gene desert (Figure 3A). Again, this tendency was also observed for the brain; 90% of *Hoxd4* contacts mapped to the telomeric side with digit material ($p = 1.1 \times 10^{-12}$) versus 74% when brain tissue was used ($p = 1.2 \times 10^{-3}$; Figure 3B).

In brain, both *Hoxd13* and *Hoxd4* displayed numerous peaks of interaction within the entire *HoxD* cluster (Figure 3C). In contrast, the interaction profile of *Hoxd13* in digits was limited to the centromeric half of the gene cluster. Likewise, *Hoxd4* contacts were mostly restricted to the telomeric part of the cluster (Figure 3C). These complementary 4C profiles thus matched the boundary between expressed (*Hoxd13* to *Hoxd10*) and nonexpressed (*Hoxd8* to *Hoxd1*) genes in developing digits. They could also be superimposed to the epigenetic status of the gene cluster since, consistent with previous studies (Bracken et al., 2006, Lee et al., 2006b, Boyer et al., 2006), tri-methylation of histone H3 at lysine 27 (H3K27me3) covered the gene cluster in brain (Figure 3C), whereas only low levels of H3K4me3, a mark associated with transcriptional activation (Bernstein et al., 2005), were scored. In contrast, digits displayed complementary histone methylation profiles, with H3K4me3 decorating the transcribed region (Figure 3C), whereas H3K27me3 marks covered the silent part of the cluster.

Regulatory Islands in the Centromeric Gene Desert

We focused on the most significant *Hoxd13* interaction peaks (with $p < 10^{-8}$; Figure S4A) and identified five islands within the *Atp5g3-Lnp* gene desert, which together concentrated the majority of these signals as well as the highest enrichments (16 out of 24 peaks with enrichment > 4; Figure 4A; I to V). Some of these islands also contacted *Hoxd13* in brain, yet with lower frequencies. We confirmed the contacts between *Hoxd13* and all five islands in digits by using 3C (Figure S4), whereas brain samples revealed interactions with islands I, II and V only. The frequency of these latter interactions was lower than in digits, suggesting they are more labile or occur in fewer cells.

We asked whether these islands could contact each others and thus selected additional starting points for 4C analysis. When island I was used, located 700 kb upstream *Hoxd13*, significant interactions were scored with sequences located mostly on the telomeric side, up to the *HoxD* cluster, overlapping with the *Hoxd13* interaction domain and thus showing opposite directionalities in the interaction profiles (Figure S4). Consistent with our previous results, islands I, IV and Prox strongly interacted with the *HoxD* cluster in digits (multiple peaks with enrichment > 4; Figure 4B). Within the cluster, contacts were strikingly restricted to those *Hoxd* genes transcribed in digits (Figure 4C). Also, the contacts experienced either by Prox, islands I or IV in developing digits overlapped with *Hoxd13* interacting regions (Figure 4B) since more than 50% of their respective peaks (enrichment > 3) matched the *Hoxd13* contacts. The Prox and *Hoxd13* profiles were highly related, and islands I and IV also contacted the other centromeric islands as well as the GCR, with various frequencies (Figure 4D). While these results do not rule out a dynamic system of pair-wise interactions, they suggest a more global association of these various elements with each other to form a specific architecture in developing digits.

In the brain, different profiles were observed. We did not detect interaction between island IV and the *HoxD* cluster, whereas both Prox and island I displayed weak contacts (Figure 4C). Interactions between various islands were also more restricted than in digits, suggesting lower frequencies in contacts (Figures 4B and 4E). Some of the interactions observed in digits were nevertheless clearly present in the brain, such as between Prox and island II or between island I and island V, and are thus independent of gene activity.

Analyses of Candidate Regulatory Elements

The five islands interacting with *Hoxd13* include many noncoding elements conserved throughout various vertebrate species (Figure 5A). We analyzed the distribution of H3K4me1 and H3K27Ac in digits, two chromatin marks associated with enhancer elements or with active enhancers and promoters, respectively (Heintzman et al., 2007, 2009; Creyghton et al., 2010; Rada-Iglesias et al., 2011). The two marks had a similar distribution and were widely enriched in the gene desert (Figure 5A and S5). We looked for the presence of RNA polymerase II (RNAPII) in digits and found it mostly within H3K4me1 and H3K27Ac decorated regions (34 out of 37 peaks).

These profiles largely overlapped with the contacts involving *Hoxd13*, with 63% of *Hoxd13* interaction peaks mapping to H4K4me1 positive regions and 47% being decorated by both histone marks ($p = 3.4 \times 10^{-3}$, Fisher's Exact Test; Figures 5A and S5). In particular, the interaction islands were densely decorated with H3K4me1 and H3K27Ac and many intergenic RNAPII-associated sequences were found over these same regions (20 out of 37 peaks, $p = 5.6 \times 10^{-3}$). This clustering of H3K4me1, H3K27Ac, RNAPII and *Hoxd13* interacting peaks was specific, as these regions were devoid of H3K27me3 and usually displayed only marginal enrichment for H3K4me3 (data not shown).

The same analyses using the brain sample revealed much reduced distributions over the gene desert, as compared to digits (Figure S5). About 40% of the areas positive for H3K4me1 in digits were also decorated in the brain sample and a few regions were scored in brain only. Several regions contacting *Hoxd13* in both digits and brain were enriched for H3K4me1 in both tissues, although the domains were shorter and less enriched in the brain (Figure 5B and S5). Interacting regions marked with H3K4me1 in digits but not in brain included island IV (Figure 5C) as well as the Prox element (Figure 5D). In

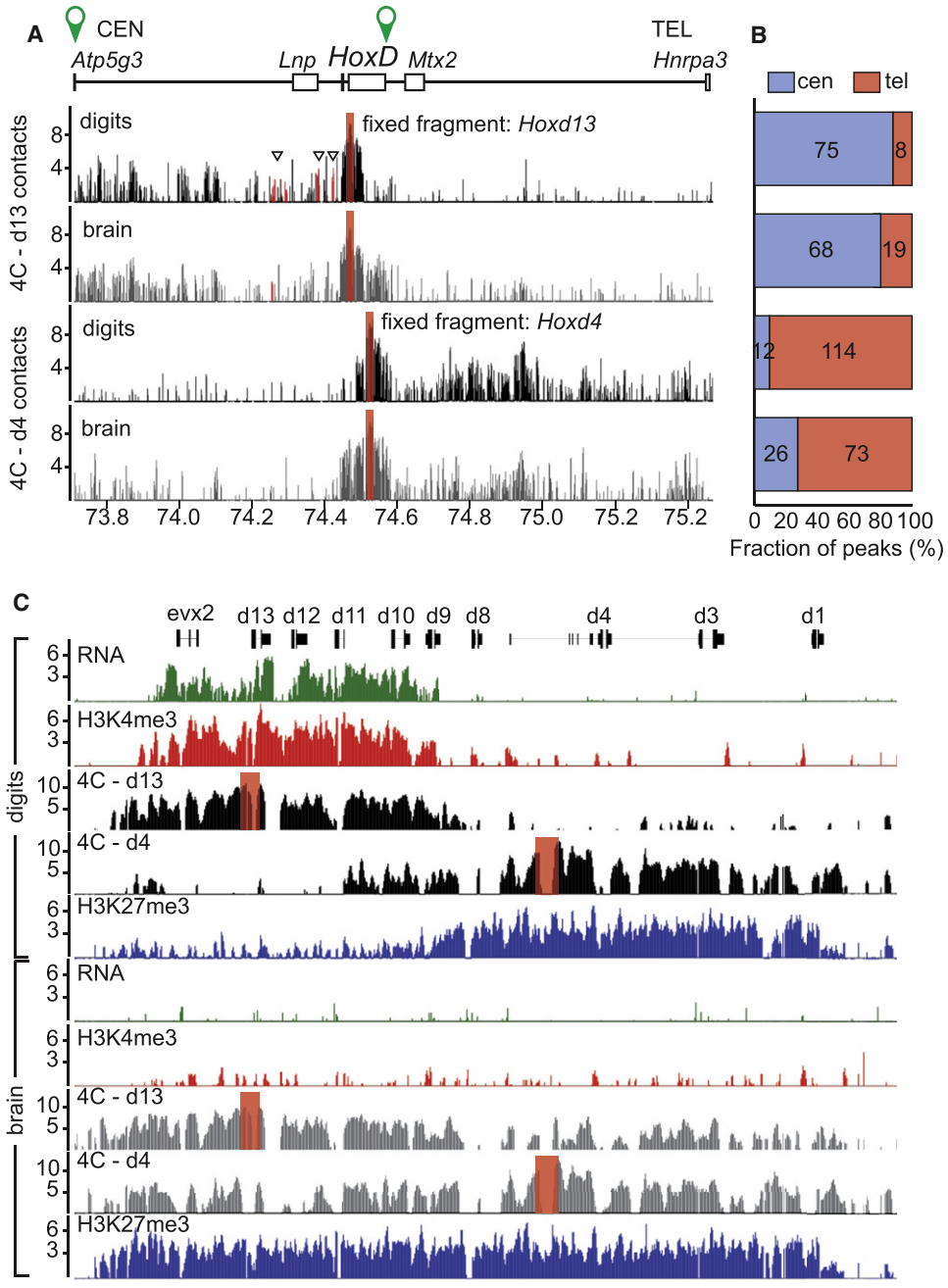

Figure 3. 3D Organization of the Whole *HoxD* Locus in Developing Digits

(A) 4C analysis with a fixed fragment (red bar) identified interactions from *Atp5g3* to *Hnrpa3*. Profiles are shown for *Hoxd13* (top) in digits (black) and brain (gray), and for *Hoxd4* (bottom) in the same tissues. The x axis shows chromosomal coordinates in megabases (UCSC 2006 assembly, mm8) and the y-axes are $\log_2$ ratio of 4C-amplified/input DNA intensity. Open arrowheads point to the GCR, the *Lnp* promoter and Prox, from left to right and the associated peaks are in red. Open green arrows on the top delineate the centromeric sub-region dispatched in Figures 4 and 5.

(B) Percentage of significant interaction peaks on either the centromeric (blue), or telomeric (red) side of the cluster, for the profiles shown in (A). Contacts within the gene cluster itself are excluded. The numbers of peaks are given within the rectangles.

(C) Active and inactive chromatin domains within the *HoxD* cluster in digits, with brain as control. The viewpoints for 4C are indicated with red rectangles. The y axis indicates the $\log_2$ ratio of cDNA/genomic DNA or ChIP-enriched/input signal intensity.

See also Figure S3.

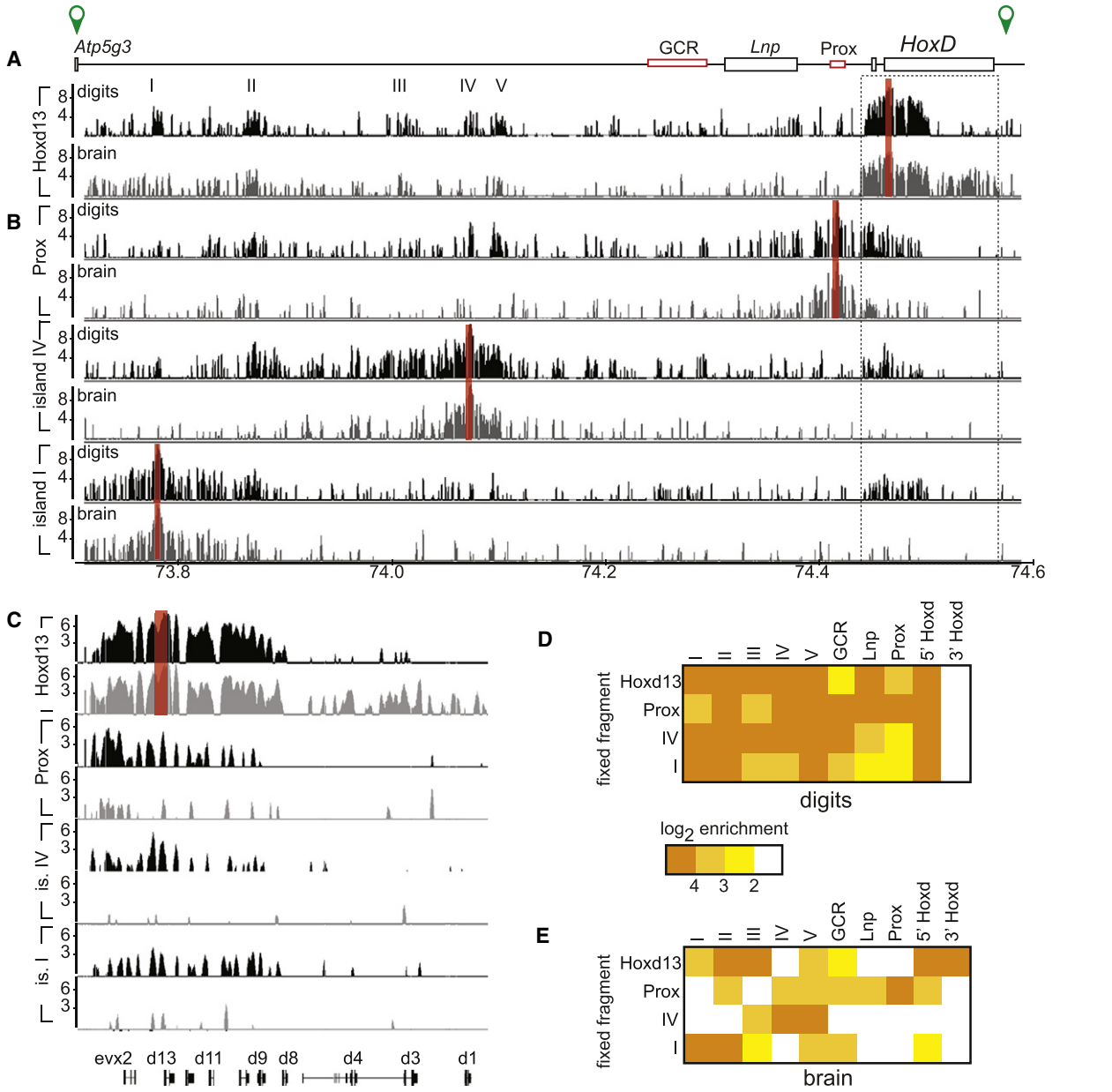

Figure 4. 3D Organization of the Centromeric Gene Desert

(A) Interactions profiles between *Hoxd13* (red bar) and centromeric sequences in digits (black) and brain (gray). Islands of interactions are labeled I to V.

(B) Top to bottom: interaction profiles, using Prox and islands IV and I as viewpoints (red bars), in digits and brain.

(C) Enlargement of the *HoxD* cluster, corresponding to dashed boxes in panel (A). Prox and islands I and IV specifically contact the active part of the cluster in digits. Weaker interactions occur in the brain for Prox and island I.

(D and E) Summary of the contacts within the centromeric region. The color of each tile indicate signal enrichment versus input over a given element. (D) Mutual interactions take place between the different elements in developing digits. (E) A subset of these contacts is also observed in the brain.

See also Figure S4.

contrast, only few regions enriched either in H3K27Ac, or in RNAPII were found outside annotated genes in the brain sample. One clear overlap between limb- and brain-enriched regions matched the CsB of the GCR (Figure 5D), maybe caused by the presence of regulatory elements involved in *Lnp* expression in the brain (Spitz et al., 2003).

Based on both their profiles of histone modifications and their phylogenetic footprint, four regions within the islands were cloned upstream of a *β-globin/LacZ* lentivirus-based reporter to evaluate their enhancer activities in vivo. Six out of 14 embryos transgenic for the island I-derived sequence (tg1; Figure 5A) displayed *LacZ* staining in the developing limb, including

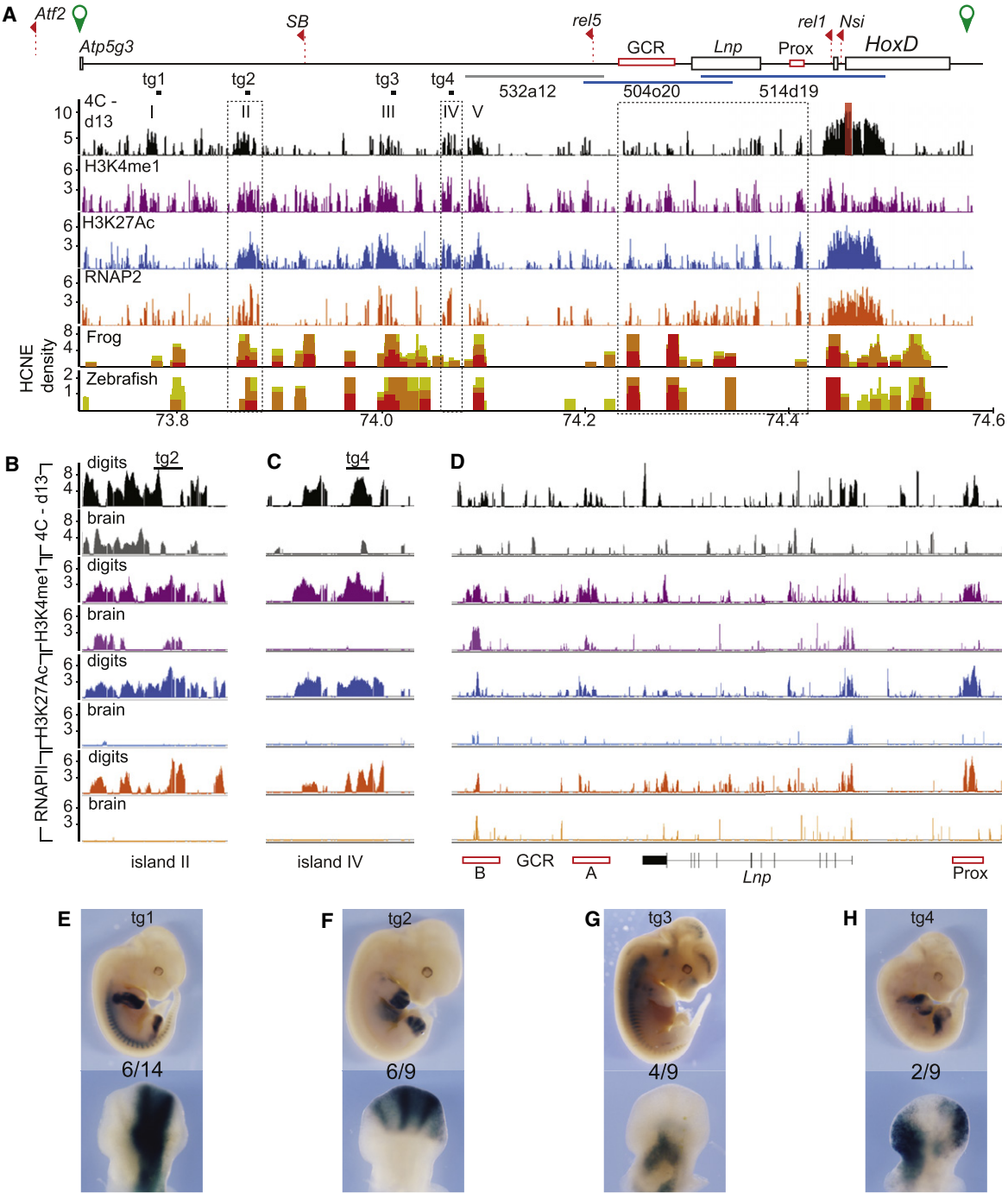

Figure 5. Potential Regulatory Elements Are Located in the Gene Desert

(A) Top to bottom: interactions profiles between *Hoxd13* and DNA fragments in the gene desert (black), H3K4me1 (magenta) and H3K27Ac (light blue) profiles and distribution of bound RNAPII (orange), in developing digits. The densities of highly conserved noncoding elements (HCNE) are plotted below. The locations of *loxP* sites used for deletions (see Figure 6) are indicated on the top (red arrowheads) as well as the BAC clones tested in former transgenic assays (Spitz et al., 2003; Gonzalez et al., 2007). BACs able to activate the reporter gene in digits are in blue, whereas a negative BAC is in gray. Four DNA fragments tested in lentivirus-mediated transgenic assays (tg1 to tg4) are shown as black rectangles.

(B–D) Enlargement of the dashed-boxed areas shown in panel (A), with corresponding profiles in digits and brain. Most RNAPII and H3K27Ac peaks are specific for digits.

(E–H) Transgenic analysis of fragments isolated from islands I to IV. (E–G) Numbers refer to embryos positive for the pattern displayed over the total number of transgenics. (H) Out of nine transgenics, three embryos showed LacZ staining, two with distinct patterns in distal limb.

See also Figure S5.

digits III, IV, and occasionally V (Figure 5E). The island II-derived tg2 element elicited a pattern almost identical to the expression of posterior *Hoxd* genes (6 out of 9 embryos; Figure 5F). In contrast, the tg3 sequence (island III) generated a reproducible signal in the trunk and parts of the proximal limb (4 out of 9 transgenic embryos; Figure 5G) yet not directly related to *Hoxd* gene expression. Two out of 9 embryos transgenic for a segment of island IV displayed distinct patterns in distal limb buds, suggesting it may also activate transcription in a *Hoxd*-like pattern (tg4; Figure 5H).

Serial Deletions of Regulatory Islands

We engineered a set of targeted deletions including and flanking the centromeric gene desert (Figure 6). Breakpoints were right upstream *Hoxd13* (*Nsi*; van der Hoeven et al., 1996), between *Evx2* and the Prox element (*rel1*; Kondo and Duboule, 1999), upstream the GCR (*rel5*), 300 Kb centromeric from *rel5* (*SB*, Ruf et al., 2011) and within the *Atf2* gene (Shah et al., 2010) close to the extremity of the gene desert (Figure 6A). Each deletion was balanced with a chromosome carrying a deletion of *Hoxd8* to *Hoxd13* [the Del(*8-13*) allele] such that only the expression of *Hoxd* genes in *cis* with the various deletions was monitored.

Removing the GCR and Prox elements along with *Lnp* [Del(*rel1-rel5*)] had surprisingly little effects on *Hoxd13* expression at E12.5. mRNAs level was down to 60% of wild-type (Table S1), with a full loss of expression in presumptive digit I. At birth, a shortening of digit V with missing middle phalange was observed (Figure 6B; arrowhead). *Evx2*, *Hoxd12*, and *Hoxd11* were also affected, to a lesser extent, whereas *Hoxd10* levels were similar to wild-type. *Hoxd* genes could thus be expressed at fairly high levels in the absence of both the GCR and Prox elements. Del(*rel5-SB*) removed 300 kb of the gene desert and also induced subtle effects, with an expression of *Hoxd13* and *Hoxd12* corresponding to about 70% of wild-type levels (Table S1). The phenotype at birth was nearly identical to wild-type, except for malformations of digit I (the thumb), though with incomplete penetrance (Figure 6C). Del(*SB-Atf2*) removed the most distant part of the gene desert and led to a loss of *Hoxd13* expression in the anterior part of the limb bud, including both digit I and part of digit II (Figure 6D). This was also observed for *Hoxd12*, *Hoxd11*, and *Hoxd10* (Figure S6B) and induced a shortening of digit II at birth, with a missing phalange. The expression levels of *Lnp*, *Evx2*, and 5′ *Hoxd* genes were half of wild-type levels (Table S1).

The 550 kb large compound Del(*Nsi-SB*) deletion induced a stronger reduction of *Hoxd13* expression throughout the distal limbs (Figure 6E). Expression was down to about one third of wild-type level and the phenotype at birth involved a shortening of both digits II and V (Figure 6E). A more dramatic downregulation of *Hoxd* genes was scored after deleting the entire gene desert, from *rel5* to *Atf2* (Figure 6F). Expression was about 20% of wild-type level (Table S1) and was limited to a faint signal in the posterior part of the hand plate. All digits were malformed at birth, with two phalanges only. This downregulation concerned the distal limb exclusively, for neither the proximal limb domain, nor the expression in the trunk were affected in these embryos (Figure S6). This deletion illustrated the moderate importance of both the GCR and Prox sequences, under full physiological conditions, thus pointing to a crucial role for the gene desert in this digit regulation. Finally, we removed the 830 kb large piece of DNA sequences from *HoxD* until *Atf2*, and distal

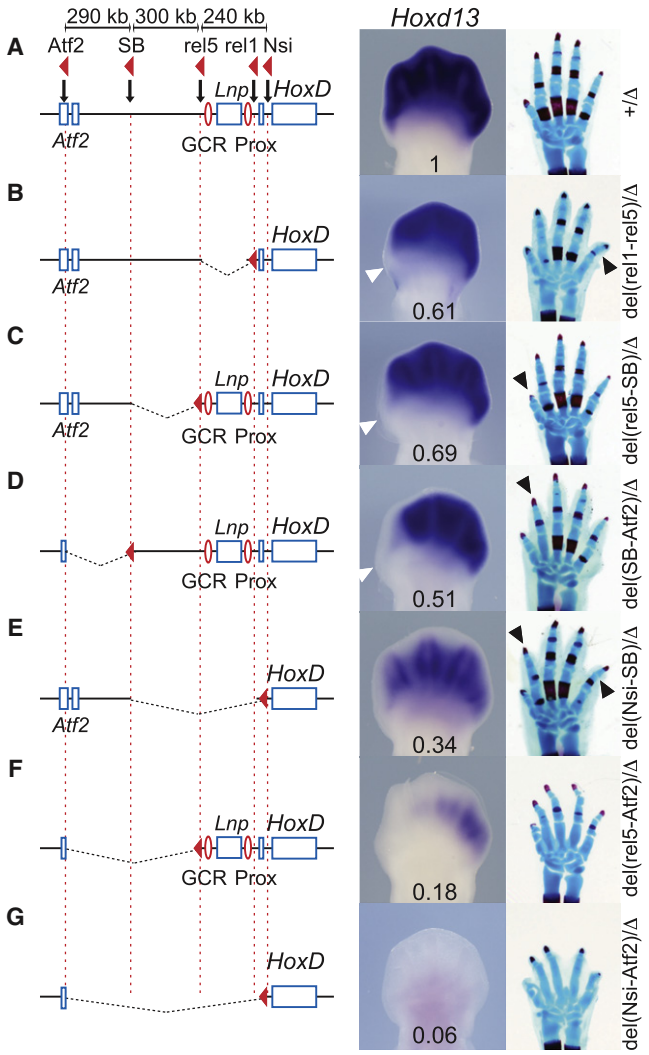

Figure 6. Serial Deletion Analysis of the Centromeric Gene Desert

Each panel represents a different mouse stock, with the deletion shown on the left, *Hoxd13* expression in the middle and a skeleton at birth on the right. Relative expression levels (RT-qPCR) are indicated under each expression pattern.

(A) Wild-type chromosome, with the position of the various loxP sites (red arrowheads).

(B) Deletion of both the GCR and Prox elements. The white arrowheads points to the future thumb.

(C) Deletion of the proximal half of the gene desert.

(D) Deletion of the distal half of the gene desert.

(E) The larger Del(*Nsi-SB*) deletion induces further decrease in *Hoxd13* expression.

(F) Deletion of the entire gene desert, with *Hoxd13* expressed at low levels, posteriorly.

(G) Deletion of the gene desert, together with the GCR and Prox, completely abolishes *Hoxd13* expression in digits. Black arrowheads point to phenotypic alterations.

See also Figure S6 and Table S1.

expression of *Hoxd13* to *Hoxd10* was fully abrogated. Accordingly, the neonatal phenotype was comparable to the Del(*8-13*) situation (Figure 6G). Therefore, several regions on the centromeric gene desert are required, in a complementary and partially redundant fashion, for gene activation in developing digits.

DISCUSSION

Transgenic analyses have suggested a critical role for both the GCR and Prox sequences in *Hoxd* genes activation during digit development (Gonzalez et al., 2007). While we now document the physical association of these enhancers with *Hoxd* genes, our data indicate that they are not sufficient for the full transcriptional outcome, in their endogenous context. Such results may reflect compensatory mechanisms at work in vivo. It also suggests that transgenic analyses should be interpreted with caution, as copy number and the stability of the reporter gene product may lead to overestimation of the transcriptional outcome. Similar concerns were raised in the case of shadow enhancers in *Drosophila* (Hong et al., 2008), where apparently redundant regulatory elements can maintain reliable expression patterns in sub-optimal conditions and thus contribute to the robustness of the systems (Frankel et al., 2010; Perry et al., 2010).

A Desert Landscape

The regulatory landscape contributing to *Hoxd* gene expression in developing digits is substantially larger than previously thought. Our series of centromeric deletions revealed that several regions distributed over 800 kb, participate in the activation of the target *Hoxd* genes. Only a deletion of the entire gene desert fully abolished gene transcription and the phenotypes of mice carrying these deletions indicated that distinct regions are only partially redundant with one another. Consistently, sequences contacted by *Hoxd13* in digit cells are mostly spread throughout this gene desert, up to the *Atp5g3* gene. When the most distant island contacted by *Hoxd13* was used as starting point, it mostly contacted sequences located in between *Atp5g3* and the *HoxD* cluster, rather than sequences located further centromeric, suggesting that this DNA interval forms a 3D domain distinct from its surrounding chromosomal regions.

This gene desert, present in all sequenced vertebrate genomes, contains range of highly conserved noncoding elements (Lee et al., 2006a). Such deserts are rarely interrupted by chromosomal rearrangements and tend to be linked to genes controlling embryonic development, suggesting they are required for large-scale regulation (Ovcharenko et al., 2005). In this case, chromatin signatures usually associated with transcriptional enhancers were over-represented. Our genetic and biochemical evidence define the *Atp5g3-Lnp* gene desert as an unusually large regulatory module, critical for *Hoxd* gene transcription in developing digits. While evolutionary conservation of gene deserts may reflect the presence of multiple regulatory modules associated with pleiotropic functions (e.g., Nobrega et al., 2003) we show here that the entire gene desert is used to fine-tune and ensure a single expression specificity.

3D Organization of the *HoxD* Landscape in Digits

In digits, the transcriptionally active *Hoxd13* strongly associated with centromeric sequences, whereas a silent gene, located on the 3′ part of the gene cluster, interacted mainly with telomeric regions. This dichotomy extended to the gene cluster itself, where active genes occupy a 3D domain distinct from inactive genes, unlike in nonexpressing cells where interactions are observed throughout the gene cluster (Eskeland et al., 2010). These patterns of interactions, which are paralleled by histone modifications, likely reflect a fixed and stable demarcation between active and repressed genes in developing digits, in contrast to the dynamic transition observed between such chromatin domains during trunk development (Soshnikova and Duboule, 2009). Our 4C results now indicate that in developing digits, such chromatin domains correspond to distinct 3D domains. The organization of the *HoxA* cluster in human fibroblasts also shows interactions between active genes, yet not between inactive loci (Wang et al., 2011).

Regulatory "Archipelagos"

The spatial organization of the *HoxD* landscape in digits is more complex than anticipated (Montavon et al., 2008). Multiple elements, spread like islands over a large desert, are brought to the vicinity of *Hoxd13 via* chromatin looping. In digits, these islands contact each other, pointing to multiple and simultaneous interactions between distant elements (Figure 7). We emphasize that a more dynamic system of transient interactions cannot be ruled out. In such a case, transient interactions would also occur between islands, rather than only between enhancers and promoters. A subset of these long-range contacts occurs at low frequency in the brain and is thus not directly associated with transcription. A less elaborate structure may thus take place as a default or poised condition. One may speculate that a few additional digit-specific interactions may initiate transcription, after recruitment of chromatin-modifying factors and RNAPII to the active chromatin loops. This possibility may explain the accumulation of global regulations within these gene deserts. In this scenario, evolution of novel enhancers would merely require one or a few more tissue-specific factors ('regulatory priming'; Gonzalez et al., 2007).

Transcription of *Hoxd* genes in digits integrates the collective activities of several regulatory elements. While some of these sequences did activate transcription in digits on their own, others may play a more structural role. 'Regulatory archipelagos' such as the one we characterize here may be numerous in vertebrate genomes and are different from other reported large scale regulatory controls at work e.g., at the *β-globin* locus, where various elements span a much shorter chromosomal segment (about 130 kb) and do not overlap with a gene desert (Tolhuis et al., 2002), or at the *Shh* locus, where activation in limb buds requires the association with a single remote enhancer, whose deletion abolishes transcription (Sagai et al., 2005; Amano et al., 2009).

Relevance to Human Syndromes and the Evolution of Digits

This regulatory archipelago provides an explanation to the molecular etiologies of various genetic syndromes where rearrangements affect the integrity of this particular gene desert in

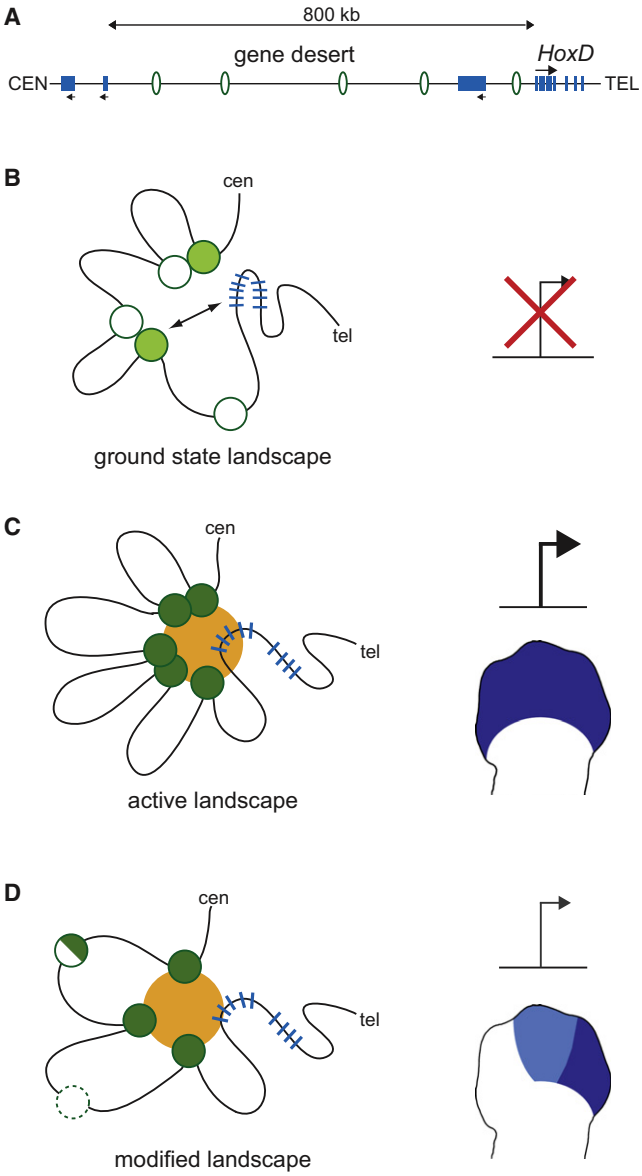

Figure 7. A Regulatory Archipelago Controls *Hoxd* Gene Expression in Digits

(A) Map of the regulatory landscape, covering approximately 800 kb upstream the *HoxD* cluster, including the *Atp5g3-Lnp* gene desert. Multiple regulatory islands (green ovals) are required for *Hoxd* gene activation in digits. These islands may either have enhancer activity or serve as anchor points.

(B–D) Various conformations of the landscape (left), with schematic representations of the transcriptional outputs and distribution of *Hoxd* gene products in the autopod domain (right). (B) When *Hoxd* genes are not expressed, the landscape is in a spatial ground state involving interactions between a subset of regulatory islands, some of which also contact the *Hoxd13* locus. Some islands may display chromatin signatures typical of enhancers (light green). These contacts are however insufficient to activate transcription. (C) In digits, additional contacts are formed, leading to a fully active conformation paralleled by further changes in histone marks covering the islands (dark green) and the recruitment of RNAPII to active chromatin loops. This architecture ensures a strong expression of *Hoxd13* throughout the whole autopod region. (D) Various alteration in the structure of the archipelago, for example in the sequence of the islands, their spacing or relative order, could modify both the amount and spatial distribution of *Hoxd* gene products, thus providing a basis for morphological or pathological variations to occur. Although this model suggests simultaneous contacts, a more dynamic process is also possible. Islands are depicted schematically and do not reflect the behavior of individual elements reported in this work.

human patients. For instance, microdeletions within this desert are associated with malformations resembling *HOXD13* mutations, even when the *HOXD* cluster itself is not affected (see Mitter et al., 2010). Also, a balanced translocation with a breakpoint within the gene desert was associated with severe digit anomalies (Dlugaszewska et al., 2006). While this latter rearrangement does not interrupt the GCR-*HOXD* linkage, it removes upstream islands, like our *rel5-Itga6* inversion. These variations likely affect the conformation of the locus, leading to modified transcriptional outputs.

This archipelago may also help understand the evolution of tetrapod digits. Distal limb morphologies are much less constrained than their proximal counterparts (Hinchliffe, 1991) and the size, shape and number of digits display high variability among species and between fore- and hindlimbs. This large gene desert could be the target of numerous evolutionary alterations or modifications, which could all slightly modify both the global transcriptional output of the system, as well as the spatial distribution of *Hoxd* gene products within the developing autopod. Conversely, its redundant and complementary nature makes this system particularly robust and the distal phase of *Hoxd* gene expression is indeed remarkably resilient to mutations of genes controlling limb morphogenesis (e.g., te Welscher et al., 2002; Verheyden et al., 2005). The buffering effect of complementary control elements may have been selected as a mean to stabilize the existence of *a* distal structure, rather than that of a given digital formula. Via additive inputs, the progressive construction of this archipelago may have accompanied the selection of a sufficient expression level for *Hoxd13* throughout the whole autopod domain, a strict requirement for the proper morphogenesis of the limb extremities.

EXPERIMENTAL PROCEDURES

Mouse Strains

The Del(*8-13*) allele is described in Tarchini et al. (2005). The insertion of the *Hoxd9LacZ* transgene at the *rel5* position (chr.2: 47222892 on NCBI build 36, mm8) followed homologous recombination in ES cells (see Extended Experimental Procedures). The inversion (*rel5-Itga6*) was generated by STRING (Spitz et al., 2005), using the *rel5-loxP* site and a *loxP* site inserted in the *Itga6* gene (Gimond et al., 1998). Recombinant offspring with both *loxP* sites in *cis* were crossed with *Hprt-Cre* mice (Tang et al., 2002). Centromeric deletions were produced by TAMERE (Hérault et al., 1998). The parental *loxP* sites were: *Nsi* (van der Hoeven et al., 1996), *rel1* (Kondo and Duboule, 1999), *rel5* (this work), *SB* (insertion 176599b; Ruf et al., 2011) and *Atf2* (Shah et al., 2010). Mice with a *loxP* site within *Atf2* were kindly provided by Drs N. Jones and W. Breitwieser from the Patterson Institute for Cancer Research, UK. Each allele was verified by Southern blotting and by sequencing. Genotyping was performed by PCR analysis (see Extended Experimental Procedures).

X-Gal Staining, In Situ Hybridization, and Skeletal Preparation

Detection of β-galactosidase reporter activity and in situ hybridization were performed according to standard protocols. Probes were: *Hoxd10* and

Hoxd11 (Gérard et al., 1996); *Hoxd12* (Izpisúa-Belmonte et al., 1991); and *Hoxd13* (Dollé et al., 1991). For skeletal preparation, newborns were stained with standard Alcian blue/Alizarin red protocols.

Reverse-Transcription Quantitative PCR Analyses

Presumptive digits were dissected from E12.5 embryos and stored in RNAlater reagent (QIAGEN) before genotyping. RNA was isolated from individual embryos using the RNeasy microkit (QIAGEN). 500 ng of RNA was reverse-transcribed using random primers and SuperScript III RT (Invitrogen). cDNA was PCR-amplified using SYBR green containing qPCR master mix (Invitrogen) with a CFX96 Real-Time System (Bio-Rad). A mean quantity was calculated from triplicate reactions for each sample. Expression changes were normalized to *Rps9*. Primers used were as described (Montavon et al., 2008).

3C Analysis

3C analysis was performed as described (Hagège et al., 2007). Presumptive digits and brains were dissected from E12.5 embryos, dissociated by collagenase, and fixed in 2% formaldehyde for 10 min at room temperature. Nuclei were stored at −80°C until genotyped. Pools of 16 digit samples or two brains were digested with BglII (New England Biolabs) and ligated in diluted conditions to promote intramolecular ligations. A control template was generated by digesting and religating BACs covering the region as well as the control *Ercc3* locus. 3C and control templates were PCR-amplified using qPCR master mix (Invitrogen) and double-dye oligonucleotide probes (5′FAM, 3′BHQ). Reactions were performed in triplicates and each PCR was repeated three times. Relative crosslinking frequencies were calculated after normalization with quantities calculated for the control template as well as for the control *Ercc3* locus (Hagège et al., 2007). At least two independant samples were analyzed for each condition. BAC clones and probes and primers sequences are listed in the Extended Experimental Procedures and Table S2.

4C Analysis

4C templates were generated as for 3C, using *Dpn*II. After ligation and purification, the sequences ligated to the fragment of interest were amplified by inverse PCR as described (Simonis et al., 2006). 200 ng of 4C template were amplified per reaction, using AmpliTaq DNA polymerase (Applied Biosystems ; see Extended Experimental Procedures for primer sequences). For each condition, 16 reactions were pooled and purified using QIAGEN PCR clean-up kit, fragmented and labeled using GeneChip WT Double-Stranded DNA Terminal Labeling Kit (Affymetrix) and hybridized to either custom-made (Soshnikova and Duboule, 2009) or chromosomes 2, X, and Y (Affymetrix) tiling arrays. Arrays were processed according to manufacturer's instructions. For each tissue and fragment of interest, two independent samples were analyzed.

ChIP-Chip

Digits and brains were dissected from E12.5 embryos, fixed in 1% formaldehyde for 15 min at room temperature, washed three times with cold phosphate buffer solution (PBS), and stored at −80°C. Pools of 16 digit samples or two brains were used for each experiment. ChIP was performed according to Lee et al. (2006c) using 2 μg of anti-H3K4me3 (ab8580, Abcam), H3K27me3 (17-622, Millipore), H3K4me1 (ab8895, Abcam), H3K27Ac (ab4729, Abcam), or RNAPII (8WG16, Covance) antibodies, and EZview Red protein G/A Affinity Gel (Sigma). Immunoprecipitated and whole cell extract (input) DNA were amplified using ligation-mediated PCR (Lee et al., 2006c), fragmented and labeled like 4C material and hybridized to custom tiling arrays. For each tissue and antibody, two independent ChIP-chip experiments were performed.

Transcript Profiling

Digits and brains were dissected from E12.5 embryos and stored in RNAlater reagent (QIAGEN) before genotyping. For each replicate, RNA was extracted from pools of eight digit samples or two brains using RNeasy mini-kit (QIAGEN). rRNA was depleted using RiboMinus Human/Mouse Transcriptome Isolation kit (Affymetrix). After cRNA amplification, double-stranded cDNA was generated using the GeneChip Whole Transcript Amplified Double-Stranded Target Assay kit (Affymetrix) according to manufacturer's instructions. cDNA was fragmented and labeled like 4C material and hybridized to tiling arrays. Control genomic DNA samples were fragmented with DNase I. For each tissue, two independent RNA samples were analyzed.

Tiling Array Data Analyses

Array data were quantile normalized within cDNA/genomic DNA, ChIP/input or 4C-amplified/input replicate groups and scaled to medial feature intensity of 100 using TAS software (Affymetrix). For each genomic position, a dataset was generated consisting of all (PM-MM) pairs mapping within a sliding window of 80 bp (transcriptome) or 250 bp (ChIP-chip and 4C). For 4C, only regions with a *p*-value lower than 5×10^{-4} over a minimum window of 250 bp were considered as peaks for further analysis. Average ratios were plotted along the genomic DNA sequence using Integrated Genome Browser (IGB) software (Affymetrix). Thresholding and extraction of peak coordinates were performed with IGB. See Extended Experimental Procedures.

Interspecies Sequence Comparison

The densities of highly conserved noncoding elements in mouse-human, mouse-*Xenopus* and mouse-zebrafish alignments were plotted using the Ancora Genome Browser (Engstrom et al., 2008), using a window size of 100 kb or 10 kb.

Lentivirus-Mediated Transgenesis

Candidate DNA segments were PCR-amplified from BACs using the Expand Long Template PCR system (Roche) and cloned in pRRLβLac vector. Virus production and injection into fertilized mouse oocytes was performed as described (Friedli et al., 2010). Founder embryos were collected after 12 days, stained for β-galactosidase activity, and genotyped by PCR on membrane DNA. See also Extended Experimental Procedures.

ACCESSION NUMBERS

Tiling array data have been submitted to Gene Expression Omnibus under accession number GSE31659.

SUPPLEMENTAL INFORMATION

Supplemental Information includes Extended Experimental Procedures, two tables, and six figures and can be found with this article online at doi:10.1016/j.cell.2011.10.023.

ACKNOWLEDGMENTS

We thank N. Jones and W. Breitwieser for mice; P. Descombes and the staff of the NCCR genomic platform; I. Barde and members of the EPFL transgenic core facility; S. Ruf for help with the SB mice; and G. Andrey, M. Friedli, P. Schorderet, and members of the Duboule laboratories for discussions and reagents. This work was supported by funds from the Ecole Polytechnique Fédérale, Lausanne, the University of Geneva, the Swiss National Research Fund, the National Research Center "Frontiers in Genetics," the EU program "Crescendo," and the ERC grants "Systems*Hox*.ch" (to D.D.) and "4C" (to W.D.-L). T.M. and D.D. designed all the experiments except the *rel5* allele (F.S. and D.D.). T.M., N.S., and F.S. performed the experiments, with the assistance of E.J. B.M., L.T., and F.S. provided mutant mice. W.D.-L. and E.S. assisted with the 3C technology. T.M. and D.D. wrote the manuscript with inputs from coauthors.

Received: February 11, 2011
Revised: June 11, 2011
Accepted: October 7, 2011
Published: November 23, 2011

REFERENCES

Amano, T., Sagai, T., Tanabe, H., Mizushina, Y., Nakazawa, H., and Shiroishi, T. (2009). Chromosomal dynamics at the Shh locus: limb bud-specific differential regulation of competence and active transcription. Dev. Cell *16*, 47–57.

Bernstein, B.E., Kamal, M., Lindblad-Toh, K., Bekiranov, S., Bailey, D.K., Huebert, D.J., McMahon, S., Karlsson, E.K., Kulbokas, E.J., Gingeras, T.R., et al.

(2005). Genomic maps and comparative analysis of histone modifications in human and mouse. Cell *120*, 169–181.

Boyer, L.A., Plath, K., Zeitlinger, J., Brambrink, T., Medeiros, L.A., Lee, T.I., Levine, S.S., Wernig, M., Tajonar, A., Ray, M.K., et al. (2006). Polycomb complexes repress developmental regulators in murine embryonic stem cells. Nature *441*, 349–353.

Bracken, A.P., Dietrich, N., Pasini, D., Hansen, K.H., and Helin, K. (2006). Genome-wide mapping of Polycomb target genes unravels their roles in cell fate transitions. Genes Dev. *20*, 1123–1136.

Bulger, M., and Groudine, M. (2011). Functional and mechanistic diversity of distal transcription enhancers. Cell *144*, 327–339.

Creyghton, M.P., Cheng, A.W., Welstead, G.G., Kooistra, T., Carey, B.W., Steine, E.J., Hanna, J., Lodato, M.A., Frampton, G.M., Sharp, P.A., et al. (2010). Histone H3K27ac separates active from poised enhancers and predicts developmental state. Proc. Natl. Acad. Sci. USA *107*, 21931–21936.

Dekker, J., Rippe, K., Dekker, M., and Kleckner, N. (2002). Capturing chromosome conformation. Science *295*, 1306–1311.

Dlugaszewska, B., Silahtaroglu, A., Menzel, C., Kubart, S., Cohen, M., Mundlos, S., Tumer, Z., Kjaer, K., Friedrich, U., Ropers, H.H., et al. (2006). Breakpoints around the HOXD cluster result in various limb malformations. J. Med. Genet. *43*, 111–118.

Dollé, P., Izpisúa-Belmonte, J.C., Boncinelli, E., and Duboule, D. (1991). The Hox-4.8 gene is localized at the 5′ extremity of the Hox-4 complex and is expressed in the most posterior parts of the body during development. Mech. Dev. *36*, 3–13.

Dollé, P., Izpisúa-Belmonte, J.C., Falkenstein, H., Renucci, A., and Duboule, D. (1989). Coordinate expression of the murine Hox-5 complex homoeobox-containing genes during limb pattern formation. Nature *342*, 767–772.

Engstrom, P.G., Fredman, D., and Lenhard, B. (2008). Ancora: a web resource for exploring highly conserved noncoding elements and their association with developmental regulatory genes. Genome Biol. *9*, R34.

Eskeland, R., Leeb, M., Grimes, G.R., Kress, C., Boyle, S., Sproul, D., Gilbert, N., Fan, Y., Skoultchi, A.I., Wutz, A., et al. (2010). Ring1B compacts chromatin structure and represses gene expression independent of histone ubiquitination. Mol. Cell *38*, 452–464.

Frankel, N., Davis, G.K., Vargas, D., Wang, S., Payre, F., and Stern, D.L. (2010). Phenotypic robustness conferred by apparently redundant transcriptional enhancers. Nature *466*, 490–493.

Friedli, M., Barde, I., Arcangeli, M., Verp, S., Quazzola, A., Zakany, J., Lin-Marq, N., Robyr, D., Attanasio, C., Spitz, F., et al. (2010). A systematic enhancer screen using lentivector transgenesis identifies conserved and non-conserved functional elements at the Olig1 and Olig2 locus. PLoS ONE *5*, e15741.

Gérard, M., Chen, J.Y., Gronemeyer, H., Chambon, P., Duboule, D., and Zàkàny, J. (1996). In vivo targeted mutagenesis of a regulatory element required for positioning the Hoxd-11 and Hoxd-10 expression boundaries. Genes Dev. *10*, 2326–2334.

Gimond, C., Baudoin, C., van der Neut, R., Kramer, D., Calafat, J., and Sonnenberg, A. (1998). Cre-loxP-mediated inactivation of the alpha6A integrin splice variant in vivo: evidence for a specific functional role of alpha6A in lymphocyte migration but not in heart development. J. Cell Biol. *143*, 253–266.

Godwin, A.R., and Capecchi, M.R. (1998). Hoxc13 mutant mice lack external hair. Genes Dev. *12*, 11–20.

Gonzalez, F., Duboule, D., and Spitz, F. (2007). Transgenic analysis of Hoxd gene regulation during digit development. Dev. Biol. *306*, 847–859.

Hagège, H., Klous, P., Braem, C., Splinter, E., Dekker, J., Cathala, G., De Laat, W., and Forné, T. (2007). Quantitative analysis of chromosome conformation capture assays (3C-qPCR). Nat. Protoc. *2*, 1722–1733.

Heintzman, N.D., Hon, G.C., Hawkins, R.D., Kheradpour, P., Stark, A., Harp, L.F., Ye, Z., Lee, L.K., Stuart, R.K., Ching, C.W., et al. (2009). Histone modifications at human enhancers reflect global cell-type-specific gene expression. Nature *459*, 108–112.

Heintzman, N., Stuart, R., Hon, G., Fu, Y., Ching, C., Hawkins, R., Barrera, L., Van Calcar, S., Qu, C., Ching, K., et al. (2007). Distinct and predictive chromatin signatures of transcriptional promoters and enhancers in the human genome. Nat. Genet. *39*, 311–318.

Hérault, Y., Rassoulzadegan, M., Cuzin, F., and Duboule, D. (1998). Engineering chromosomes in mice through targeted meiotic recombination (TAMERE). Nat. Genet. *20*, 381–384.

Hinchliffe, J.R. (1991). Developmental approaches to the problem of transformation of limb structure in evolution. In Developmental Patterning of the Vertebrate Limb, J.R. Hinchliffe, J.M. Hurle, and D. Summerbell, eds. (New York: Plenum Publishing Corp.), pp. 313–323.

Hong, J.W., Hendrix, D.A., and Levine, M.S. (2008). Shadow enhancers as a source of evolutionary novelty. Science *321*, 1314.

Izpisúa-Belmonte, J.C., Falkenstein, H., Dollé, P., Renucci, A., and Duboule, D. (1991). Murine genes related to the Drosophila AbdB homeotic genes are sequentially expressed during development of the posterior part of the body. EMBO J. *10*, 2279–2289.

Kmita, M., and Duboule, D. (2003). Organizing axes in time and space; 25 years of colinear tinkering. Science *301*, 331–333.

Kondo, T., and Duboule, D. (1999). Breaking colinearity in the mouse HoxD complex. Cell *97*, 407–417.

Lee, T.I., Jenner, R.G., Boyer, L.A., Guenther, M.G., Levine, S.S., Kumar, R.M., Chevalier, B., Johnstone, S.E., Cole, M.F., Isono, K., et al. (2006b). Control of developmental regulators by Polycomb in human embryonic stem cells. Cell *125*, 301–313.

Lee, T.I., Johnstone, S.E., and Young, R.A. (2006c). Chromatin immunoprecipitation and microarray-based analysis of protein location. Nat. Protoc. *1*, 729–748.

Lee, A.P., Koh, E.G., Tay, A., Brenner, S., and Venkatesh, B. (2006a). Highly conserved syntenic blocks at the vertebrate Hox loci and conserved regulatory elements within and outside Hox gene clusters. Proc. Natl. Acad. Sci. USA *103*, 6994–6999.

Mitter, D., Chiaie, B.D., Lüdecke, H.-J., Gillessen-Kaesbach, G., Bohring, A., Kohlhase, J., Caliebe, A., Siebert, R., Roepke, A., Ramos-Arroyo, M.A., et al. (2010). Genotype-phenotype correlation in eight new patients with a deletion encompassing 2q31.1. Am. J. Med. Genet. A. *152A*, 1213–1224.

Montavon, T., Le Garrec, J.-F., Kerszberg, M., and Duboule, D. (2008). Modeling Hox gene regulation in digits: reverse collinearity and the molecular origin of thumbness. Genes Dev. *22*, 346–359.

Nelson, C.E., Morgan, B.A., Burke, A.C., Laufer, E., DiMambro, E., Murtaugh, L.C., Gonzales, E., Tessarollo, L., Parada, L.F., and Tabin, C.J. (1996). Analysis of Hox gene expression in the chick limb bud. Development *122*, 1449–1466.

Nobrega, M.A., Ovcharenko, I., Afzal, V., and Rubin, E.M. (2003). Scanning human gene deserts for long-range enhancers. Science *302*, 413.

Ovcharenko, I., Loots, G.G., Nobrega, M.A., Hardison, R.C., Miller, W., and Stubbs, L. (2005). Evolution and functional classification of vertebrate gene deserts. Genome Res. *15*, 137–145.

Perry, M.W., Boettiger, A.N., Bothma, J.P., and Levine, M. (2010). Shadow enhancers foster robustness of Drosophila gastrulation. Curr. Biol. *20*, 1562–1567.

Rada-Iglesias, A., Bajpai, R., Swigut, T., Brugmann, S.A., Flynn, R.A., and Wysocka, J. (2011). A unique chromatin signature uncovers early developmental enhancers in humans. Nature *470*, 279–283.

Ruf, S., Symmons, O., Uslu, V.V., Dolle, D., Hot, C., Ettwiler, L., and Spitz, F. (2011). Large-scale analysis of the regulatory architecture of the mouse genome with a transposon-associated sensor. Nat. Genet. *43*, 379–386.

Sagai, T., Hosoya, M., Mizushina, Y., Tamura, M., and Shiroishi, T. (2005). Elimination of a long-range cis-regulatory module causes complete loss of limb-specific Shh expression and truncation of the mouse limb. Development *132*, 797–803.

Shah, M., Bhoumik, A., Goel, V., Dewing, A., Breitwieser, W., Kluger, H., Krajewski, S., Krajewska, M., Dehart, J., Lau, E., et al. (2010). A role for ATF2 in regulating MITF and melanoma development. PLoS Genet. *6*, e1001258.

Simonis, M., Klous, P., Splinter, E., Moshkin, Y., Willemsen, R., De Wit, E., Van Steensel, B., and De Laat, W. (2006). Nuclear organization of active and inactive chromatin domains uncovered by chromosome conformation capture-on-chip (4C). Nat. Genet. *38*, 1348–1354.

Soshnikova, N., and Duboule, D. (2009). Epigenetic Temporal Control of Mouse Hox Genes in Vivo. Science *324*, 1320–1323.

Spitz, F., Gonzalez, F., and Duboule, D. (2003). A global control region defines a chromosomal regulatory landscape containing the HoxD cluster. Cell *113*, 405–417.

Spitz, F., Herkenne, C., Morris, M., and Duboule, D. (2005). Inversion-induced disruption of the Hoxd cluster leads to the partition of regulatory landscapes. Nat. Genet. *37*, 889–893.

Tang, S.H., Silva, F.J., Tsark, W.M., and Mann, J.R. (2002). A Cre/loxP-deleter transgenic line in mouse strain 129S1/SvImJ. Genesis *32*, 199–202.

Tarchini, B., Huynh, T.H., Cox, G.A., and Duboule, D. (2005). HoxD cluster scanning deletions identify multiple defects leading to paralysis in the mouse mutant Ironside. Genes Dev. *19*, 2862–2876.

Tarchini, B., and Duboule, D. (2006). Control of Hoxd genes' collinearity during early limb development. Dev. Cell *10*, 93–103.

te Welscher, P., Zuniga, A., Kuijper, S., Drenth, T., Goedemans, H.J., Meijlink, F., and Zeller, R. (2002). Progression of vertebrate limb development through SHH-mediated counteraction of GLI3. Science *298*, 827–830.

Tolhuis, B., Palstra, R.J., Splinter, E., Grosveld, F.G., and De Laat, W. (2002). Looping and interaction between hypersensitive sites in the active beta-globin locus. Mol. Cell *10*, 1453–1465.

Tschopp, P., and Duboule, D. (2011). A Regulatory 'Landscape Effect' Over the HOXD Cluster. Dev. Biol. *351*, 288–296.

van der Hoeven, F., Zàkàny, J., and Duboule, D. (1996). Gene transpositions in the HoxD complex reveal a hierarchy of regulatory controls. Cell *85*, 1025–1035.

van Steensel, B., and Dekker, J. (2010). Genomics tools for unraveling chromosome architecture. Nat. Biotechnol. *28*, 1089–1095.

Verheyden, J.M., Lewandoski, M., Deng, C., Harfe, B., and Sun, X. (2005). Conditional inactivation of Fgfr1 in mouse defines its role in limb bud establishment, outgrowth and digit patterning. Development *132*, 4235–4245.

Wang, K.C., Yang, Y.W., Liu, B., Sanyal, A., Corces-Zimmerman, R., Chen, Y., Lajoie, B.R., Protacio, A., Flynn, R.A., Gupta, R.A., et al. (2011). A long noncoding RNA maintains active chromatin to coordinate homeotic gene expression. Nature *472*, 120–124.

Zakany, J., and Duboule, D. (2007). The role of *Hox* genes during vertebrate limb development. Curr. Opin. Genet. Dev. *17*, 359–366.

Zhao, Z., Tavoosidana, G., Sjolinder, M., Gondor, A., Mariano, P., Wang, S., Kanduri, C., Lezcano, M., Sandhu, K.S., Singh, U., et al. (2006). Circular chromosome conformation capture (4C) uncovers extensive networks of epigenetically regulated intra- and interchromosomal interactions. Nat. Genet. *38*, 1341–1347.